Environmental Science and Pollution Research (2023) 30:18546–18562
https://doi.org/10.1007/s11356-022-23359-0

RESEARCH ARTICLE

RGO nanosheet wrapped β-phase $NiCu_2S$ nanorods for advanced supercapacitor applications

Narthana Kandhasamy[1] · Laguduva K. Preethi[2] · Devendiran Mani[3] · Lukasz Walczak[4] · Tom Mathews[5] · Rajendran Venkatachalam[1,6]

Received: 29 June 2022 / Accepted: 26 September 2022 / Published online: 10 October 2022

Abstract

A new integration strategy of transition metal sulfide with carbon-based materials is used to boost its catalytic property and electrochemical performances in supercapacitor application. Herein, crystalline reduced graphene oxide (rGO) wrapped ternary metal sulfide nanorod composites with different rGO ratios are synthesized using hydrothermal technique and are compared for their physical, chemical, and electrochemical performances. It is found that their properties are tuned by the weight ratios of rGO. The electrochemical investigations reveal that β-$NiCu_2S$/rGO nanocomposite electrode with 0.15 wt.% of rGO is found to possess maximum specific capacitance of 1583 F g^{-1} at current density of 15 mA g^{-1} in aqueous electrolyte medium. The same electrode shows excellent cycling stability with capacitance retention of 89% after 5000 charging/discharging cycles. The reproducibility test performed on $NiCu_2S$/rGO nanocomposite electrode with 0.15 wt.% of rGO indicates that it has high reproducible capacitive response and rate capability. Thus, the present work demonstrates that the β-$NiCu_2S$/rGO nanocomposite can serve as a potential electrode material for developing supercapacitor energy storage system.

Keywords Ternary metal sulfide · Reduced graphene oxide · Hydrothermal · Electrochemical behavior · Energy storage · Supercapacitor

Introduction

Supercapacitors have attracted major attention as an energy storage device because of their ability to deliver excellent power density, fast charging rates with slow discharging time, and superior cycling stability (Ghosh and Pumera 2021; Lin et al. 2021), thus making it a suitable choice to combat the increasing demand for portable devices and electric vehicles. The properties of materials being used as the electrodes highly influence the performance of a supercapacitor. Various materials in the form of oxides (Zhai et al.2020), nitrides (Maity et al. 2020), hydroxides, sulfides (Wang et al. 2020a, b), phosphates (Iqbal et al. 2021c), polymers (Khanam et al. 2020), etc. have been studied for their supercapacitor performances (Hsu et al. 2021; Kang et al. 2022). Among them, binary sulfide materials based on transition metals (Lin et al. 2021) such as NiS, Ni_3S_4 (Guan et al. 2017; Gou et al. 2017), CoS (Liu et al. 2015; Aloqayli et al. 2017), MnS (Pujari et al. 2016; Tang et al. 2015a), MoS_2 (Karade et al. 2016; Ghosh et al. 2021), Cu_2S, and Cu_7S_4 (Yue et al. 2021; Gao et al. 2021; Zhang et al. 2021d) have been shown to possess enhanced supercapacitor performances. However, these

Responsible Editor: George Z. Kyzas

✉ Rajendran Venkatachalam
veerajendran@gmail.com

[1] Centre for Nano Science and Nanotechnology, K.S. Rangasamy College of Technology, Tiruchengode, Tamil Nadu 637215, India

[2] Centre for Nanoscience and Nanotechnology, Sathyabama Institute of Science and Technology (Deemed to Be University), Chennai, Tamil Nadu 600119, India

[3] Central Instrumentation Laboratory, Vels Institute of Science Technology and Advanced Studies (VISTAS), Chennai, Tamil Nadu 600117, India

[4] Science & Research Division, PREVAC Sp. Z O.O, 44-362 Rogow, Poland

[5] Surface and Nanoscience Division, Materials Science Group, Indira Gandhi Centre for Atomic Research, HBNI, Kalpakkam 603102, India

[6] Department of Physics, Dr. N. G. P. Arts and Science College, Coimbatore, Tamil Nadu 641048, India

binary sulfides offer low energy density, which hinders its practical application. In order to improve energy density as well as to obtain superior supercapacitor performances, ternary metal sulfides are preferred over binary sulfides due to their excellent optical property, high catalytic efficiency, and superior electrical conductivity (Liu et al. 2018). Unlike transition metal oxides, the reports on the discussion of supercapacitor performances of ternary metal sulfides are limited. Recently, it has been observed that, compared with transition metal oxides, transition metal sulfides offer unique stoichiometric compositions, enhanced redox reaction, and higher specific capacitance due to different valence states and crystal structure (Niu et al. 2021; Wang et al. 2018). Particularly, nickel-copper-sulfide nanomaterials have drawn increasing interest as a result of their superior redox characteristics and high theoretical specific capacitance arising as a result of Cu atom offering different oxidation states when combined with high electrochemically active Ni element (Li et al. 2021a). They are also cost-effective and least polluting. Thus, integrating Ni and Cu results in high electrochemical properties (Shinde et al. 2021; Kiey and Hasanin 2021) and, when combined with sulfur, the material Ni-Cu-S gives rise to high conductivity, narrow band gap, better ionic diffusivity, and large anion polarizability, contributing largely towards enhanced supercapacitor performances (Iqbal et al. 2021b). Apart from the above-mentioned advantages, metal sulfides in general suffer from poor long-term cycling stability due to the insulating nature of sulfur. Also, the volume expansions of sulfides and thermodynamically unstable and oxidizing nature of sulfides are the most common problems when dealing with metal sulfides in supercapacitor application (Iqbal et al. 2021a).

On the other hand, carbon materials derivatives such as graphene, graphene oxide, reduced graphene oxide, carbon nanotubes, and nanocarbon have been synthesized in different routes (Gurzęda et al. 2017; Trikkaliotis et al. 2020; Deng et al. 2022; Peng et al. 2022; Ghosh et al. 2021; Ojha et al. 2021) and extensively studied for various energy and environmental applications such as batteries (Liu et al. 2022; Alidoost et al. 2022; Xu et al. 2022a), solar cell (Bandara et al. 2022; Murugadoss et al. 2016; Murugadoss et at. 2015), supercapacitors (Arora et al. 2022; Chen et al. 2022; Shokry et al. 2022; Reina et al. 2022; Yibowei et al. 2021), oxygen reduction reaction (Xu et al. 2022b; Karanfil et al. 2022; Singla et al. 2021), photocatalytic/electrocatalytic water splitting (Antony et al. 2015; Shah et al. 2022; Zhu et al. 2022; Purabgola et al. 2022; Truong et al. 2022), and pollutant removal (Oliveira et al 2019; Tan et al. 2016). Especially, carbon-based materials (Zhang et al. 2021c) as electrodes for supercapacitor have acquired potential attraction due to their excellent electrochemical properties, high active surface area, and good conductivity resulting in efficient charge storage with high power density though energy density is limited (Iqbal et al. 2021a; González and Colet 2019). In order to overcome the shortcomings of metal sulfides in supercapacitor application, metal sulfides have been made composites with carbon-based materials and studied for their supercapacitor performances. Recently, cobalt sulfide was made composite with nitrogen doped carbon derived from zeolitic imidazolate frameworks-67 using chemical vapor deposition technique (Wang et al. 2022) which were proposed to have advanced electrode performances in supercapacitor application. The composite electrode exhibited specific capacitance of 789 F g^{-1} at current density of 1 A g^{-1} with a rate capacity of 80.2% under a current density of 20 A g^{-1}. The fabricated capacitor with the CoS-carbon composite obtained a high energy density of 32.8 Wh kg^{-1} with the power density of 620 W kg^{-1} and possessed 89.2 of capacity retention after 10,000 charge-discharge cycles at current density of 5 A g^{-1}. On the other hand, Mn^{2+} doped CoS_2-carbon nanotube composites synthesized by wet-chemical approach (Agboola et al. 2022) were found to have excellent electrical conductivity (0.063 S cm^{-1}) with specific capacitance of 603 F g^{-1} at 5 mV s^{-1} and 82.2% capacitance retention. It was proposed that the CNT support increased the electrical conductivity of Mn-CoS_2, reduced its aggregation which facilitated the ease transfer of ions during electrochemical reactions. Similarly, Ramesh et al. (2022) fabricated $NiCo_2S_4$-metal organic framework nanostructured multiwalled carbon nanotube composites which were found to possess a specific capacitance of 455 F g^{-1} at 1 A g^{-1} with excellent capacitance retention of 98.43% after 10,000 cycles. Recently, Rana et al. (2022) studied the electrochemical behavior of rGO wrapped chromium sulfide nanoplates on nickel foam for supercapacitor application. They found that the robust and porous structure of the electrode facilitated the electrolyte diffusion and thus showcased outstanding electrochemical performance by exhibiting a specific capacitance of 2563.12 F g^{-1} at 5 mV s^{-1} with energy density of 87.50 Wh kg^{-1} and power density of 1607 W kg^{-1} at 2.0 mA cm^{-2}. The fabricated electrode also obtained a stability up to 1000 cycles which was attributed to the outstanding electrical conduction provided by rGO between the nickel foam and Cr_2S_3. Further, the ternary composite such as Ti_3C_2/carbon nanotubes/$MnCo_2S_4$ electrodes designed by Dang et al. (2022) which showed gravimetric capacitance of 823 F g^{-1} at a current density of 1 A g^{-1} with 63.5% specific capacity retention at 5 A g^{-1} and had excellent cycling stability of 94.09% after 5000 cycles. The high performance of this electrode is due to the conductive network provided by Ti_3C_2/CNT hybrid sheets which efficiently accommodate the volume swelling of $MnCo_2S_4$. Thus because of extraordinary electrochemical behavior, facile synthesis, economical, and low toxicity of carbon materials, they are made composite with other materials to obtain the desired supercapacitor performance.

Likewise, it has been found that ternary metal compounds offer the best supercapacitor performances when made composites with different carbon materials due to high surface area offered by carbon materials that improves the redox reactions (Li et al. 2021b; Liu et al. 2021), thus enhancing the conductivity, stability, and electrochemical activity (Tang et al. 2015b; Zhang et al. 2021a). Among different carbon materials, rGO has been widely studied and found to be one of the most promising supports for nanomaterials in supercapacitor applications (Patil et al. 2021). For example, Hoa et al. (2021) exhibited the electrochemical supercapacitor performances of needle-like RGO/$NiCo_2S_4$ aerogel synthesized using hydrothermal technique. The prepared aerogel electrode showed a high specific capacity of 813 F g^{-1} in the 3 M KOH aqueous electrolyte at a current rate of 1.5 A g^{-1}, due to its high porosity and conductive nature. The asymmetric supercapacitor of RGO/$NiCo_2S_4$//RGO delivered a specific capacitance of 45.3 F g^{-1} at 1 A g^{-1} and capacitance retention of 84.3% after 2000 cycles. It also delivered high energy density of 40.3 Wh kg^{-1} at 375 W kg^{-1} and a power density of 26.2 kW kg^{-1} at 3.7 kWh kg^{-1}. Similarly, Xu et al. (2020) synthesized $NiMoS_4$/RGO lamella structure by a hydrothermal approach and got a specific capacity of 124 mAh g^{-1} at 1 A g^{-1}. The fabricated $NiMoS_4$/RGO//activated carbon device possessed an excellent energy density of 63 Wh kg^{-1} at power density 1125 W kg^{-1} with stable capacitance retention of 81% after 5000 cycles, owing to the high chemical activity of Ni with better conductive support provided by Mo and RGO. Another study reported the synthesis of sandwich-like $NiCo_2S_4$/RGO using vacuum filtration method (Wu et al. 2018), exhibiting specific capacity of 1000.5 F g^{-1} at 1 A g^{-1} and the asymmetric supercapacitor (ASC) fabricated with $NiCo_2S_4$/RGO//AC hybrid electrode delivered high energy density of 15.4 Wh kg^{-1} and power density 2227.3 W kg^{-1} with cycling stability of 80.5% over 5000 cycles, due to the increase in interlayer spacing, thus aiding the efficient penetration and diffusion of ions. Recently, manganese cobalt sulfide/rGO nanocomposites synthesized through dispersion method by Tung et al. (2022) were found to exhibit specific capacitance of 3812.5 F g^{-1} at 2 A g^{-1} and 1780.8 F g^{-1} at a high current density of 50 A g^{-1} with the capacitance retention over 92% after 22,000 cycles at 50 A g^{-1}. It was observed that the presence of rGO decreased the charge transfer resistance and enhanced ion exchange during the electrochemical studies. To the best of our knowledge, there are no reports which demonstrate the electrochemical performances of ternary Ni-Cu sulfide/rGO nanocomposites. Due to the unique supercapacitor properties of NiCuS and rGO materials, fabricating β-NiCuS/rGO composites and using them for supercapacitors application could be a promising strategy for improving the performances of energy storage devices (Zhang et al. 2020).

In order to understand the performances of β-NiCuS/rGO composites for supercapacitor application, herein we synthesized β-$NiCu_2S$ (NC) and β-$NiCu_2S$/0.05 wt.% of rGO (NCR-1), β-$NiCu_2S$/0.1 wt.% of rGO (NCR-2), and β-$NiCu_2S$/0.15 wt.% of rGO (NCR-3) nanocomposites via one-step hydrothermal approach. The structure, morphology, composition, and chemical state of synthesized pristine β-$NiCu_2S$ and composites are characterized using X-ray diffraction (XRD), Fourier transform infrared (FTIR) spectroscopy, Raman spectroscopy, field emission scanning electron microscope (FESEM), and X-ray photoelectron spectroscopy (XPS). Electrochemical studies are carried out with three-electrode cell configuration. The fabricated β-$NiCu_2S$ (NC) and different composites NCR-1, NCR-2, and NCR-3 are also evaluated in detail for their supercapacitor performances.

Experimental procedure

Materials

All chemicals used here are analytical grade and used without further purification. Nickel chloride ($NiCl_2{\cdot}6H_2O$), copper chloride ($CuCl_2{\cdot}6H_2O$), thiourea (NH_2CSNH_2), polyvinylidene difluoride (PVDF), carbon black, nickel foam (NF) and hydrazine hydrate ($N_2H_2{\cdot}H_2O$) were procured from Sigma Aldrich. N-methyl-2-pyrrolidone (NMP) was obtained from SDFCL, India. Potassium hydroxide (KOH), hydrochloric acid (HCl), deionized (DI) water, acetone, and ethanol were purchased from SRL chemicals, India.

Sample preparation

Preparation of NC nanorods

In order to prepare NC nanorods, 0.48 g $NiCl_2{\cdot}6H_2O$, 0.54 g $CuCl_2{\cdot}6H_2O$, and 1.52 g NH_2CSNH_2 were added into 40 mL DI water and continuously stirred for 30 min. After this, 20 mL of $N_2H_2{\cdot}H_2O$ was added dropwise into the above mixture and stirred for other 30 min to obtain black precipitate. The obtained transparent black precipitate was further transferred into a 100-mL autoclave and hydrothermally treated at 160 °C for 20 h. Once reaching room temperature, the sample was centrifuged with DI water and ethanol several times. The obtained final product was dried at 80 °C for 12 h. This is labeled as NC. The same procedure was repeated for the preparation of NCR-1, NCR-2 and NCR-3 composites where the stipulated amount of graphene oxide (synthesis procedure of GO is given below) was added into the black precipitate mentioned above, stirred for 30 min, and transferred to autoclave for hydrothermal treatment at 160 °C for 20 h. The GO is reduced to rGO due to the presence of hydrazine

hydrate present in the reaction mixture and hence leads to the formation of NC-rGO composites.

Preparation of graphene oxide

Modified Hummers method was followed for the synthesis of graphene oxide (GO). Graphite (10 g) and sodium nitrate ($NaNO_3$) (4 g) were mixed into 185 mL of concentrated sulfuric acid (H_2SO_4) and the reaction mixture was magnetically stirred in an ice bath for 1 h. Later, potassium permanganate ($KMnO_4$) (32 g) was added slowly into the reaction mixture while maintaining its temperature below 5 °C and the suspension was continuously stirred for 1 h. After vigorous stirring, ice bath was removed, which resulted in dark brown color solution to which deionized water was added until suspension volume reaches 500 mL, followed by addition of hydrogen peroxide (H_2O_2) (15 mL). Finally, the obtained suspension was centrifuged and washed repeatedly with water and hydrochloric acid (HCl). The product was dried at 80 °C for 24 h to obtain GO, the pH of which was found to be 5.7 after washing.

Electrode fabrication

The working electrode was fabricated using the synthesized materials by mixing them with carbon black (super P) and polyvinylidene fluoride (PVDF) (binder) in the weight ratio of 80:10:10. The above mixer was well ground and N-methyl-2-pyrrolidone (NMP) solvent was added to make it slurry. Then, the obtained black color slurry was uniformly coated on pure Ni foam (NF) and dried at 60 °C for 5 h. The dried NF was used as working electrode for supercapacitor studies. The weight of the electrode materials, coated on the Ni foam, is calculated by finding the difference of weight of Ni foam before and after slurry coating. Prior to the electrode preparation, the NF was washed with 3 M HCl, acetone, ethanol, and DI water, respectively, in an ultrasonic bath for each 10 min to eliminate NiO layer on the NF surface. The cleaned NF was dried in a vacuum oven at 60 °C for 2 h.

Material characterization

Crystalline nature and phase identifications of the as-prepared samples are carried out using powder XRD with Cu Kα radiation (D8, Bruker). The functional groups of prepared samples were investigated by FTIR spectroscopy (PerkinElmer-1600). The morphology analysis of NC and different weight ratio of rGO NCR (1–3) samples is performed by FE-SEM (JEOL 6360). A Raman spectroscopic study of the synthesized samples was carried out using Renishaw Raman spectrometer coupled with laser source of wavelength 514 nm. XPS was performed using hemispherical analyzer EA 15 (PREVAC) equipped with dual anode non-monochromatic X-ray source RS 40B1 (PREVAC). The measurements were performed using Al Kα (1486.6 eV) radiation and analyzer pass energy of 100 eV. The electron binding energy (BE) scale was calibrated at the maximum of C 1 s core excitation at 285 eV.

Electrochemical studies

The electrochemical measurements were carried out on Bio-Logic (SP-300) electrochemical workstation in a three-cell electrode configuration. The as-fabricated NF electrode was used as working electrode; saturated calomel electrode (SCE) and Pt-wire were utilized as reference and counter electrode, respectively. The electrochemical activities of the as-prepared pristine NC and ternary material composites (NCR-1, NCR-2 and NCR-3) were evaluated using cyclic voltammetry (CV), galvanostatic charge–discharge (GCD), and electrochemical impedance spectroscopic (EIS) techniques. The electrochemical performance was measured within the potential range of 0 to 0.6 V in 3 M KOH aqueous electrolyte. The specific capacitance (*SC*) of the fabricated electrode materials was estimated from the CV profiles using the following Eq. 1:

$$SC = \frac{1}{v \times m \times (\Delta V)} \int_{Vi}^{Vf} I(V)dV \quad (1)$$

where *SC* represents the specific capacitance (F/g), *v* denotes the scan rate (mV/s), *m* is the mass loading of the active material, ΔV represents the potential window (V), and $\int_{Vi}^{Vf} I(V)dV$ denotes the integral area under the CV curve. The specific capacitance (*SC*) of the fabricated electrode was calculated from the GCD curves by the following Eq. 2:

$$SC = \frac{I \times \Delta t}{m \times \Delta v} \quad (2)$$

where *SC* represents the specific capacitance (F/g), *I* denotes the current density (A), Δt is the discharge time (s), Δv represents the potential window (V), and *m* denotes the mass (g) of the active material (Narthana et al. 2021; Gholami and Arvand 2021).

To understand the reproducibility of NCR composites, four similar electrodes were fabricated using the best sample. The reproducibility of the electrodes of the best sample was conducted by analyzing CV measurements carried out at 20 mV s^{-1} and GCD measurements carried out at a current density of 15 mA g^{-1} in 3 M KOH electrolyte using electrochemical work station. The

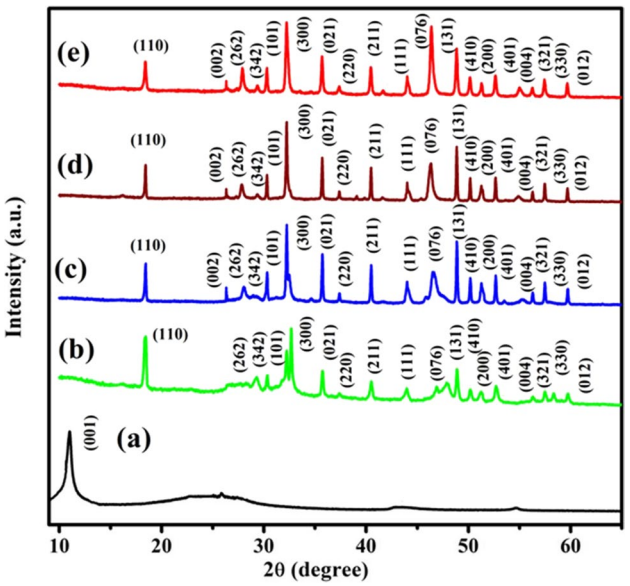

Fig. 1 XRD pattern of (**a**) GO, (**b**) NC, (**c**) NCR-1, (**d**) NCR-2 and (**e**) NCR-3

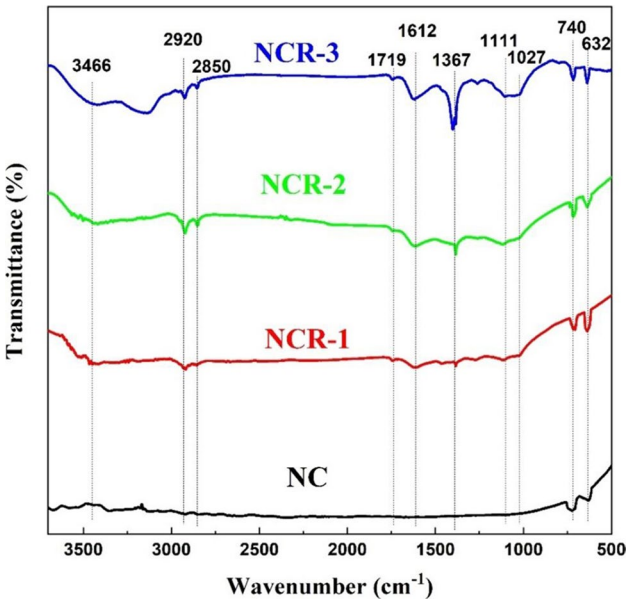

Fig. 2 FTIR spectrum of (**a**) NC, (**b**) NCR-1, (**c**) NCR-2 and (**d**) NCR-3

reproducibility of the samples was also tested by comparing GCD measurements obtained at 15, 16, 17, 18 and 20 mA g^{-1} current densities for all the four electrodes. The electrodes were thoroughly cleaned with distilled water several times, dried it and placed inside the vacuum desiccator before every measurement.

Results and discussion

The crystal phase purity of the prepared samples was evaluated by powder X-ray diffraction (PXRD) experiment, depicted in Fig. 1. The XRD spectra of all the samples (Fig. 1a, b, c, d) exhibit the diffraction peaks at 2θ angles of 18.44°, 30.33°, 32.68°, 35.73°, 37.39°, 40.49°, 48.87°, 50.17°, 52.68°, 56.29°, 57.48° and 59.76°, which can be indexed to the planes (110), (101), (300), (021), (220), (211), (131), (410), (401), (321), (330) and (012) of rhombohedral phase of β-NiS (JCPDS: 12–0041), respectively (Xie et al. 2021; Bhagwan et al. 2020). Similarly, they exhibit the diffraction peaks at 2θ angles of 27.89°, 28.09°, 29.38° and 46.63°, which can be indexed to the planes of (024), (262), (342) and (076) of orthorhombic Cu_2S, respectively (JCPDS: 12–0227) (Rahaman et al. 2020). In addition to the above diffraction planes, the XRD patterns of NCR-1, NCR-2 and NCR-3 also exhibit newer diffraction peaks at 2θ = 27.85° and 29.27°, corresponding to (024) and (342) planes of Cu_2S, the intensity of which increases as we increase the concentration of rGO. This clearly indicates that the increased rGO concentration in NCR-2 and NCR-3 nanocomposites induced a phase change in Cu_2S. The XRD of all samples possesses distinct peaks at 44° and 51.2°, which correspond to (111) and (200) peaks of Ni-Cu (JCPDS: 65–7246). Thus, from the characteristic XRD, peaks analysis indicates the formation of β-$NiCu_2S$.

The XRD graph of as synthesized graphene oxide is given in Fig. 1a. A strong peak at 2θ = 11.9° corresponding to (001) plane of GO clearly indicates that the synthesized GO is of high quality and good crystallinity (Siburian et al. 2018). There is also a weak peak present at 2θ = 26.49° that can be ascribed to the disordered character of graphitic structure caused by oxidation process and also indicates the traces of unoxidized graphite (Gurzęda et al. 2017). Whereas in Fig. 1b, c, d, the signature peak of GO (2θ = 11.9°) is totally absent and whereas the peak at 2θ = 26.3° which corresponds to the π-conjugated structure of graphene is of high intensity which clearly indicates that the added GO into the β-$NiCu_2S$ reaction mixture was completely reduced to reduced graphene oxide (rGO) after hydrothermal treatment due to the presence of hydrazine hydrate (Shoeb et al. 2021; Hu et al. 2020; Hidayah et al. 2017). In Fig. 1b, c, d, there are weak intensity peaks present at approximately 2θ = 26.32°, 42.63°, and 54.97°, which correspond to the (002), (100) and (004) reflection planes of rGO, respectively (Singh et al. 2021). It is clearly evident that the added GO into the β-$NiCu_2S$ reaction mixture is completely reduced to reduced graphene oxide (rGO) after hydrothermal treatment due to the presence of hydrazine hydrate (Shoeb

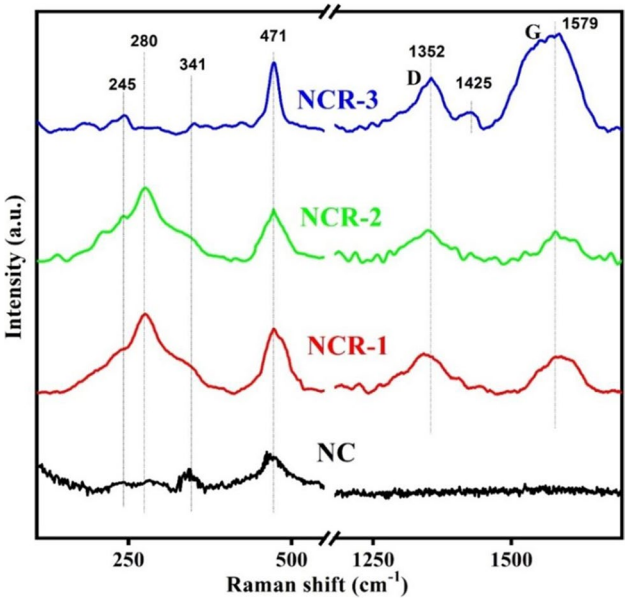

Fig. 3 Raman spectrum of (**a**) NC, (**b**) NCR-1, (**c**) NCR-2 and (**d**) NCR-3

et al. 2021; Hu et al. 2020). It can be seen that the XRD patterns of prepared nanocomposite peak has no other impurity peaks. Also, it is noticed that the intensity of the peaks increases with respect to increase in rGO composition, as evident from Fig. 1. This clearly indicates that the synthesized samples are highly pure and crystallinity increases with increase in rGO concentration. Pure and high crystalline sample can provide a fast diffusion channel for ions and promote the electrochemical reaction in supercapacitor application (Wang et al. 2019).

The FTIR spectra of the as-synthesized materials such as pristine NC and their rGO nanocomposites (NCR-1, NCR-2 and NCR-3) are shown in Fig. 2. All the samples exhibit stronger absorption bands around 632 cm^{-1} and 740 cm^{-1}, which can be ascribed to Ni–S bond vibration in c (Jansi et al. 2019) and Cu–S vibration in Cu_2S (Yu et al. 2016). The appearance of peak at 1612 cm^{-1} metal–OH stretching vibration in NCR-1 to NCR-3 samples indicates the formation of NC-rGO composites (Kamalanathan and Gopalakrishnan 2015). The peak at 3466 cm^{-1} is ascribed to the stretching vibration of O–H bonds due to the presence of moisture in all the composite samples. The absorption bands at 1738, 1367 and 1111 cm^{-1} observed in NCR-1 to NCR-3 samples can be ascribed to the stretching vibrations of C = O from carbonyls groups, carboxyl stretching C–OH of O = C–OH, and C–O alkoxy groups present in the rGO, respectively. Similarly, the characteristics rGO absorption peaks at 2920 and 2850 cm^{-1}, corresponding to C–H stretching in asymmetric and symmetric vibrations, respectively, are found to be absent in NC. As it is noticed that these characteristics rGO peaks are less in intensity in NCR-1 to NCR3 samples. This indicates the maximum reduction of GO to rGO during the hydrothermal synthesis. Among NCR samples, NCR-3 possesses slightly higher intensity characteristic peaks of rGO, which can be due to the presence of high rGO concentration. The additional peak

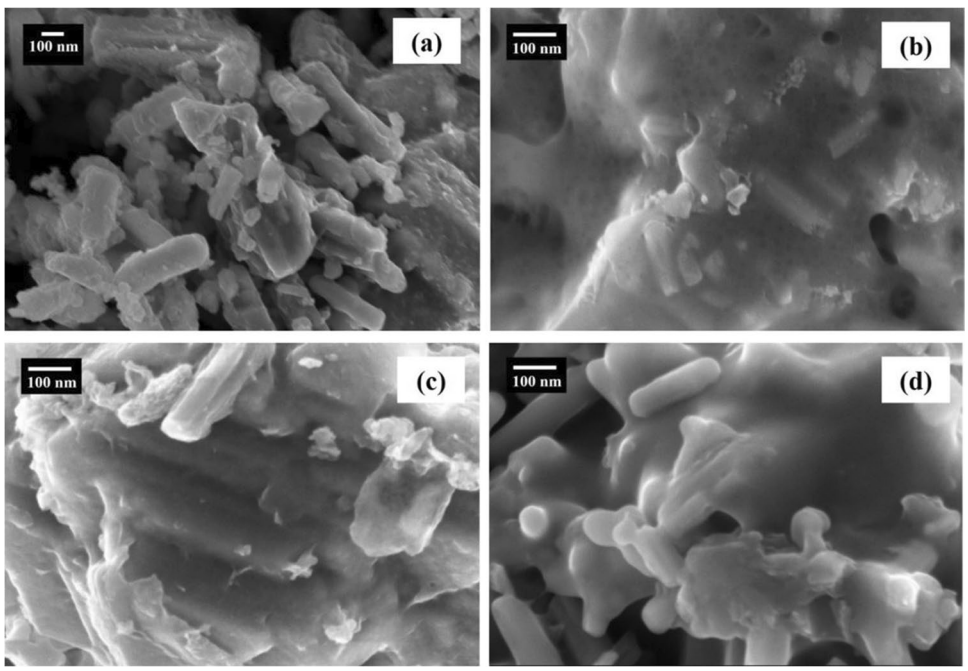

Fig. 4 FE-SEM images of (**a**) NC, (**b**) NCR-1, (**c**) NCR-2 and (**d**) NCR-3

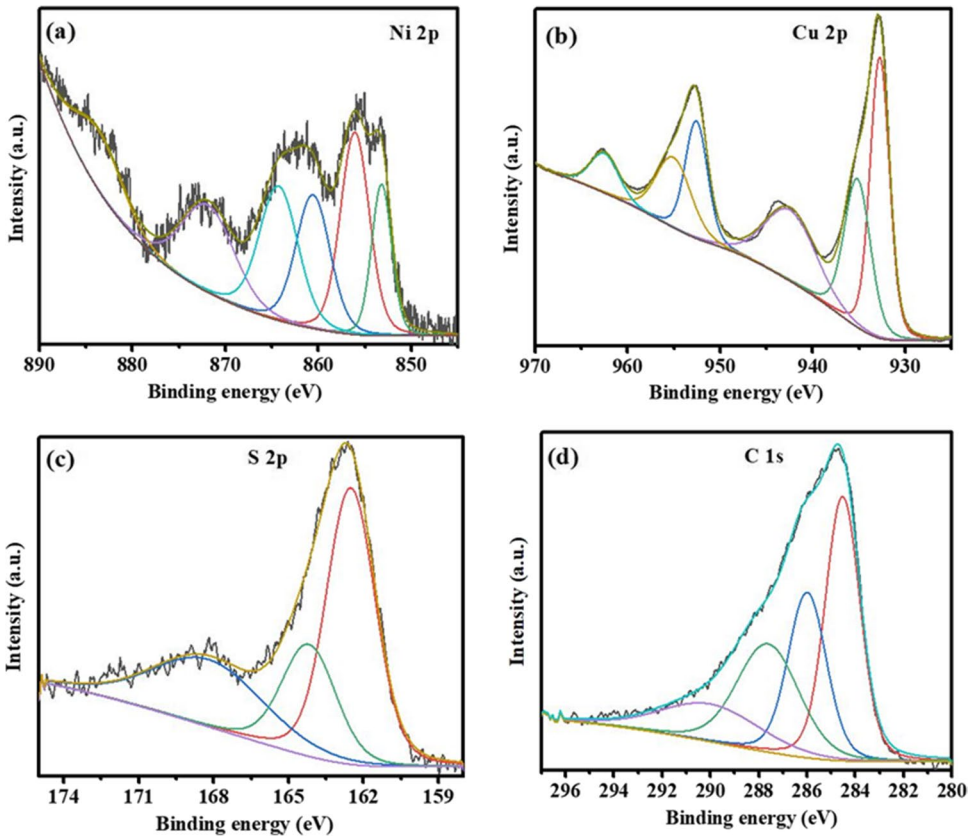

Fig. 5 XPS spectra of NCR-3 nanocomposite: (**a**) Ni 2p, (**b**) Cu 2p, (**c**) S 2p and (**d**) C1s level spectra

present at 1027 cm^{-1} corresponds to C–O stretching mode that arises from the adsorbed carbon and oxygen atom in the samples from the atmosphere (Narthana et al. 2021).

The Raman spectra of all the synthesized samples have been analyzed and presented in Fig. 3. The Raman peaks around 245 and 280 cm^{-1} correspond to β-NiS vibration (Bishop et al. 1998). These peaks are weakly present in NC and NC-3, whereas these peaks are intense in NCR-1 and NCR-2. A weak vibrational mode observed around 341 cm^{-1} present in all the samples belongs to β-NiS vibration (Li et al. 2007). On the other hand, the vibrational mode at 472 cm^{-1} corresponds to Cu_2S (Lai et al. 2010), which is present in all the samples. The difference in the characteristic bands of Raman spectra among different samples is thought to be caused by the change in the coordination state of metal ion and/or the microstructure of the NiS or Cu_2S nanoparticles, which is evident from the FESEM images in Fig. 4. Thus, the Raman analysis of all the samples confirms the presence of β-$NiCu_2S$, which is in agreement with the XRD results. The presence of rGO in the samples is analyzed using D and G bands in Raman spectra. All the composite samples have their D and G band present at 1352 cm^{-1} and 1580 cm^{-1}, whereas these peaks are absent in pristine NC sample, thus confirming the presence of rGO in composites. The D band observed at around 1352 cm^{-1} indicates the features of sp^3 defects in carbon, while the G band observed around 1579 cm^{-1} represents the in-plane vibrations of sp^2 bonded carbons (Perera et al. 2012; Rao et al. 2011). The intensity ratio of the D band to the G band (I_D/I_G) is calculated in general to study the order of defects in rGO or graphene (Perera et al. 2012). The I_D/I_G values are calculated to be 1.1, 0.95, and 0.6 for NCR-1, NCR-2 and NCR-3, respectively. It is observed that the I_D/I_G value decreases with increase in rGO concentration in the composite samples. The high I_D/I_G ratio of NCR-3 implies that the sample has lower density of defects present in rGO compared to NCR-1 and NCR-2 composites. Also, the decrease in the I_D/I_G ratio denotes the increase in the number of rGO layers (Yoon et al. 2009). This can be attributed to the increase in rGO composition in NCR-3. It is also noted that, in NCR-3, the G band is broadened, while the intensity of the D band increases slightly when compared to NCR-1 and NCR-2, which can be attributed to the significant decrease in size of the in-plane sp^2 domains (Shen et al. 2011). A weak peak at 1430 cm^{-1} in NCR-3 could be attributed to sp^3 hybridization-rich phase of amorphous carbons (Chadha et al. 2021), which may be present due to the high concentration of rGO. The results from Raman spectra analysis demonstrate the successful reduction of GO to rGO during hydrothermal treatment as well as the formation of β-$NiCu_2S$/rGO composites.

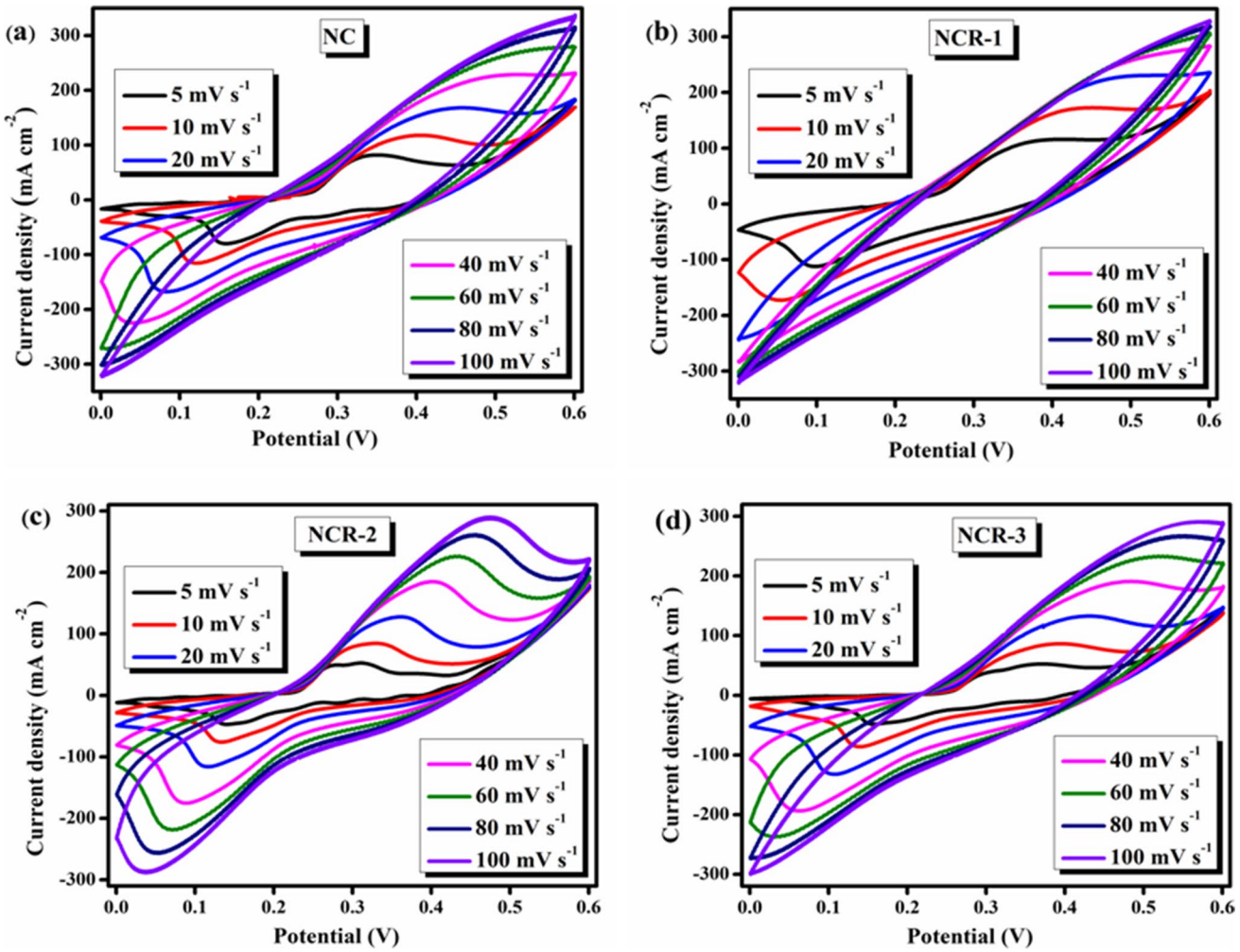

Fig. 6 CV profile of (**a**) NC, (**b**) NCR-1, (**c**) NCR-2 and (**d**) NCR-3

The morphology of as prepared pristine NC and NCR-1, NCR-2 and NCR-3 composites was analyzed using FE-SEM (Fig. 4). The SEM image of pristine NC (Fig. 4a) exhibited distinct rod like structure. Thereby in Fig. 4b, c, d, it is noticed that the β-$NiCu_2S$ nanorods are wrapped with rGO nanosheet on their surface. The rGO nanosheet wraps around β-$NiCu_2S$ nanorods increase their contact surface area, which paves way for efficient redox reaction due to enhanced charge transfer and conductivity of the composite samples. The nanorods are less visible and rGO sheet morphology is more prominent with increase in rGO weight percent as in NCR-3, indicating a dense wrap of rGO nanosheets over $NiCu_2S$ nanorods compared to NCR-2 and NCR-1 (Hu et al. 2021; Huang et al. 2021).

The wrapping of rGO nanosheets over β-$NiCu_2S$ nanorods increases their contact surface area, which paves the way for efficient redox reaction due to enhanced charge transfer and conductivity (Xu et al. 2020). The protective layers of rGO also aid in improving the material conductivity and also avert the aggregation of β-$NiCu_2S$ nanoparticles (Wang et al. 2020a). The average length and diameter of the nanorods are calculated to be 270 and 100 nm for NC, 220 and 75 nm for NCR-1, 250 and 60 nm for NCR-2 and 230 and 63 nm for NCR-3.

The chemical composition and the oxidation state of NiCuS/rGO are studied using XPS. The Ni 2p spectra of NiCuS/rGO are deconvoluted, as shown in Fig. 5a. The peaks located at 873.5 eV and 855.9 eV represent Ni $2p_{1/2}$ and Ni $2p_{3/2}$, respectively, with their satellite peaks present at 883.6, 864.7 and 860.8 eV (Beigbaghlou et al. 2018). This indicates that Ni is present in the form of Ni^{2+}. The peak at 852.9 eV is due to the presence of metallic Ni (Ni^0) on the surface (Hengne et al. 2018; Cao and Cheng 2019) due to NiCu alloy phase. The Cu spectra of the sample have Cu $2p_{3/2}$ peak at 932.8 eV and Cu $2p_{1/2}$ peak at 952.8 eV, which suggest that Cu is in the form of Cu_2S (Kar et al. 2014), which is evident from the XRD, Raman, and FTIR spectra results. The

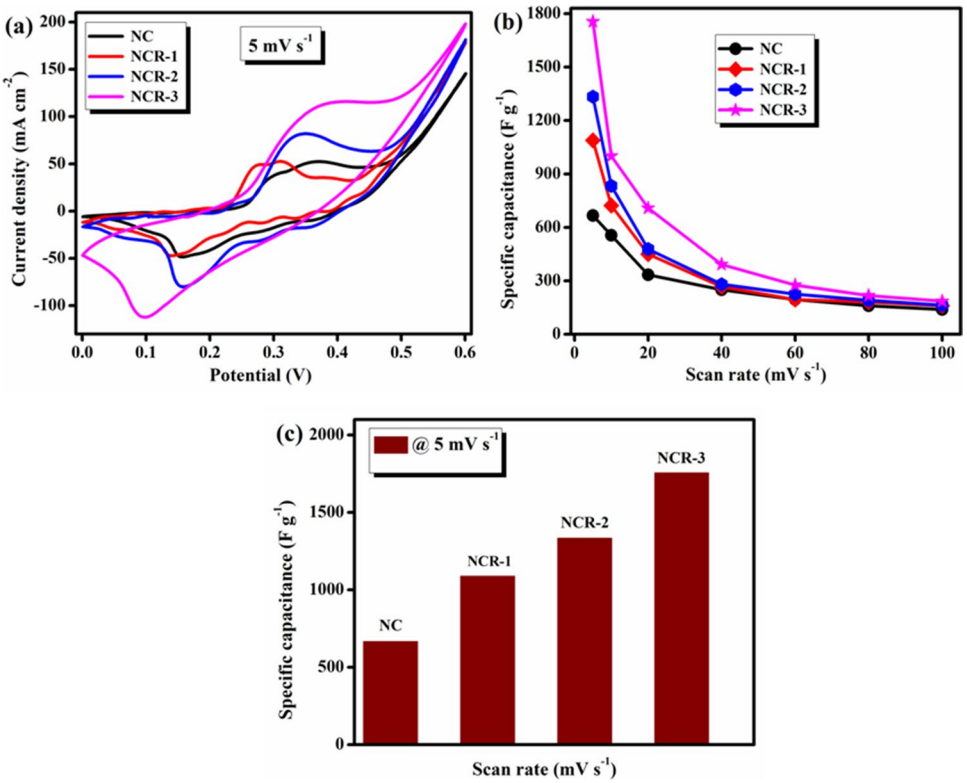

Fig. 7 (**a**) Comparison of CV profile for all fabricated samples of NC, NCR-1, NCR-2 and NCR-3 at 5 mV s^{-1}; (**b**) scan rate vs specific capacitance; and (**c**) comparison of specific capacitance of the fabricated electrodes at the scan rate of 5 mV $s.^{-1}$

deconvolution of Cu 2p spectra is presented in Fig. 5b, in which the peaks centered at 954.6 eV and 952.2 eV correspond to Cu $2p_{1/2}$, whereas the peaks centered at 934.8 eV and 932.7 eV correspond to Cu $2p_{3/2}$. The peaks centered at 962.1 eV and 942 eV are the satellite peaks of Cu 2p (Cao and Cheng 2019). In Fig. 5c, the deconvolution of S 2p spectra gives rise to three peaks, in which the peaks centered at 163.8 eV and 162.1 eV correspond to S $2p_{1/2}$ and S $2p_{3/2}$, respectively. The shake-up satellite peak present at 168.2 eV can be attributed to the presence of surface adsorbed sulfur species, such as SO_4^{2-} and HSO_4^- (Khani and Wipf 2017; Justin et al. 2019). From Fig. 5d, the presence of rGO is confirmed by analyzing the C 1 s spectra of the sample. The deconvolution of C 1 s spectra gives rise to four peaks centered at 284.5, 286, 287.6 and 290 eV, which correspond to the graphitic sp^2 hybridized graphitic carbon (C = C), the graphitic sp^2 carbon atom (C–O), the carbonyl (C = O), and the carboxyl carbon (HO–C = O), respectively, which confirm the presence of rGO in the sample (Zhang et al. 2021b).

Table 1 Calculated specific capacitance at the scan rate of 5 mV s^{-1}

Electrode materials	Scan rate (mV s^{-1})	Specific capacitance (F g^{-1})
NC	5	666.7
NCR-1	5	1088.9
NCR-2	5	1333.4
NCR-3	5	1755.6

Electrochemical performance

The electrochemical performance of electrodes prepared with NC, NCR-1, NCR-2 and NCR-3 is evaluated by CV, GCD and EIS measurements via 3-electrode cell configuration in 3 M KOH aqueous electrolyte. Figure 6 displays the cyclic voltammograms of NC, NCR-1, NCR-2 and NCR-3 electrodes performed at a scan rate of 5 to 100 mV s^{-1} in the potential range from 0.0 to 0.6 V. The CV profiles of all the fabricated electrodes exhibited a pair of redox peaks, which confirm that the charges are stored in a Faradic manner under redox reactions (Xu et al. 2020). The observed pair of oxidation and reduction peaks in Fig. 6 resulted from Ni^{2+}/Ni^{3+} and Cu^{+}/Cu^{2+} redox reactions (Wu et al. 2018). From Fig. 6a, b, c, d, it is observed that the area under the CV curves of all pristine and nanocomposite samples are increasing with increase in the sweep rate over 5 to 100 mV s^{-1} which is attributed to the minimal internal resistance at the electrode–electrolyte interface (Xie et al. 2021).

It is noticed, from the CV of NCR composite samples, that as the scan rate increases, the oxidation and reduction peaks were shifted to the higher and lower potentials, respectively. Among all the electrodes, NCR-3 shows the

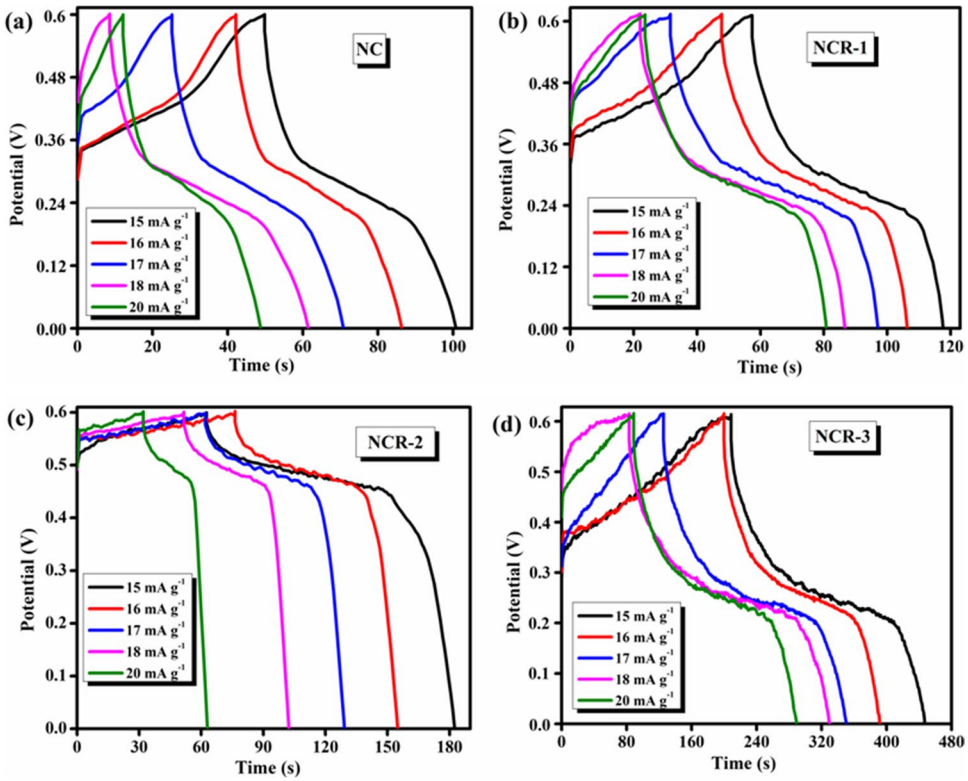

Fig. 8 GCD curves of (**a**) NC, (**b**) NCR-1, (**c**) NCR-2 and (**d**) NCR-3

largest CV area (Fig. 6d), hinting that the incorporation of rGO (0.15 wt.%) has improved the electrochemical performance of the $NiCu_2S$/rGO composite (Sabeeh et al. 2021; Ndambakuwa et al. 2021). This electrode also possessed high stability during the electrochemical process. The redox peaks of NCR-3 are observed to be high due to the high amount of rGO present in the sample compared to NCR-1 and NCR-2 (Darsara et al. 2021; Miao et al. 2020). The CV profiles of all the electrodes at 5 mV s^{-1} (Fig. 7a) are compared and it is noticed that NCR-3 exhibits larger area compared to other composite samples. The overall specific capacitances (*SC*) are calculated using Eq. 1 from Fig. 7a and displayed in Table 1.

From Table 1, it is noted that the fabricated NCR-3 electrode delivers maximum *SC* of 1755.6 F g^{-1} at 5 mV s^{-1}, which is attributed to the enhanced surface to volume ratio and efficient electron transport property due to the presence of large amount of rGO and its efficient interface with $NiCu_2S$. The *SC* values are calculated with respect to different scan rates and are plotted in Fig. 7b. It is noticed that the *SC* values are decreased when the scan rate is increased, which is because of the deficient time for the electrolyte ions to diffuse into electrode inner pores at higher scan rates (He et al. 2020). Also, it is noticed that the specific capacitance value is dependent on the rGO concentration in the samples. Among all samples, it is noticed that NCR-3 has higher specific capacitance in all scan rates compared to other composites (NCR-1 and NCR-2) and pristine NC owing to the higher rGO concentration. Also, the CV profile of NCR-3 electrode shows high specific surface-active area compared to pristine NC, NCR-1 and NCR-2, respectively, at same scan rate of 5 mV s^{-1}, as shown in Fig. 7c.

The galvanostatic charge/discharge studies are carried out for pristine NC and composite NCR-1, NCR-2 and NCR-3 electrodes in 3 M KOH electrolyte with potential window from 0.0 to 0.6 V for different current densities of 15, 16, 17, 18 and 20 mA g^{-1}, which are depicted in Fig. 8a, b, c, d. The distinct voltage plateaus in the GCD curves exhibit the battery-supercapacitor hybrid characteristics, which is consistent with the results of CV curves in Fig. 6a, b, c, d. Figure 8 shows typical supercapacitor characteristics with excellent electrochemical capacitive nature and superior electrochemical

Table 2 Calculated specific capacitance at the current density of 15 mA g^{-1}

Electrode materials	Current density (mA g^{-1})	Specific capacitance (F g^{-1})
NC	15	527
NCR-1	15	648
NCR-2	15	991
NCR-3	15	1583

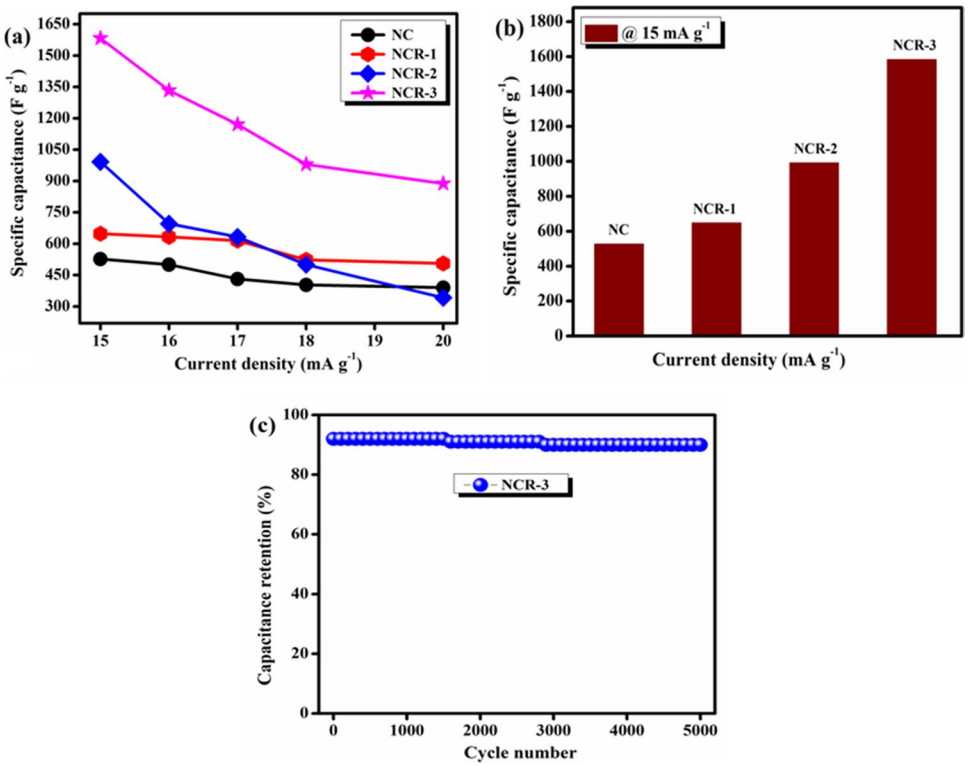

Fig. 9 GCD analysis of (**a** and **b**) specific capacitance of fabricated electrodes NC, NCR-1, NCR-2 and NCR-3 and (**c**) represent capacitance retention of NCR-3 electrode at 5000 cycles

reversibility (Gholami and Arvand 2021). Compared to pristine NC electrode (Fig. 8a), the nanocomposite NCR-1, NCR-2 and NCR-3 electrodes in Fig. 8b, c, d shows the longest charge–discharge time and highest specific capacitance, which is in good agreement with the CV results discussed above. The SCs are calculated from discharge time in corresponding GCD curves using Eq. 2, which are displayed in Table 2.

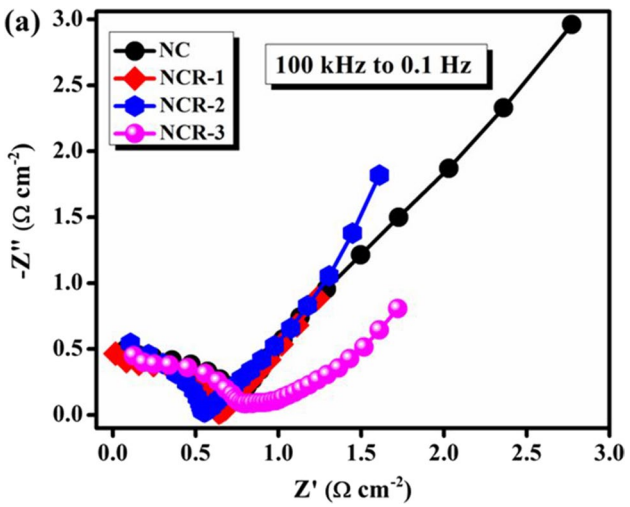

Fig. 10 EIS profile of (**a**) NC, NCR-1, NCR-2 and NCR-3

Among the electrodes, NCR-3 exhibited higher specific capacitance values, as shown in Fig. 9a, b, which is in agreement with the CV results. The stability is tested for NCR-3 electrode, which is the best performing sample, the results of which are presented in Fig. 9c. It suggests that NCR-3 retained about 89% of its initial capacitance after 5000 cycles at 18 mA g^{-1}. The cycling stability results show remarkable rate capability of composites owing to its high electrochemical stability. This is because of the increase in concentration of rGO, leading to the increase in high surface to volume ratio resulting in efficient ion transfer in the electrode/electrolyte interface (Nandhini and Muralidharan 2021; Boopathiraja et al. 2020).

The interfacial charge transport resistance of the electrolyte/electrode material interface for all the pristine and composite samples is measured using EIS-Nyquist plot

Table 3 The charge transfer resistance of synthesized samples

Electrode materials	Charge transfer resistance, Rct (Ω cm^{-1})
NC	28
NCR-1	19
NCR-2	15
NCR-3	12

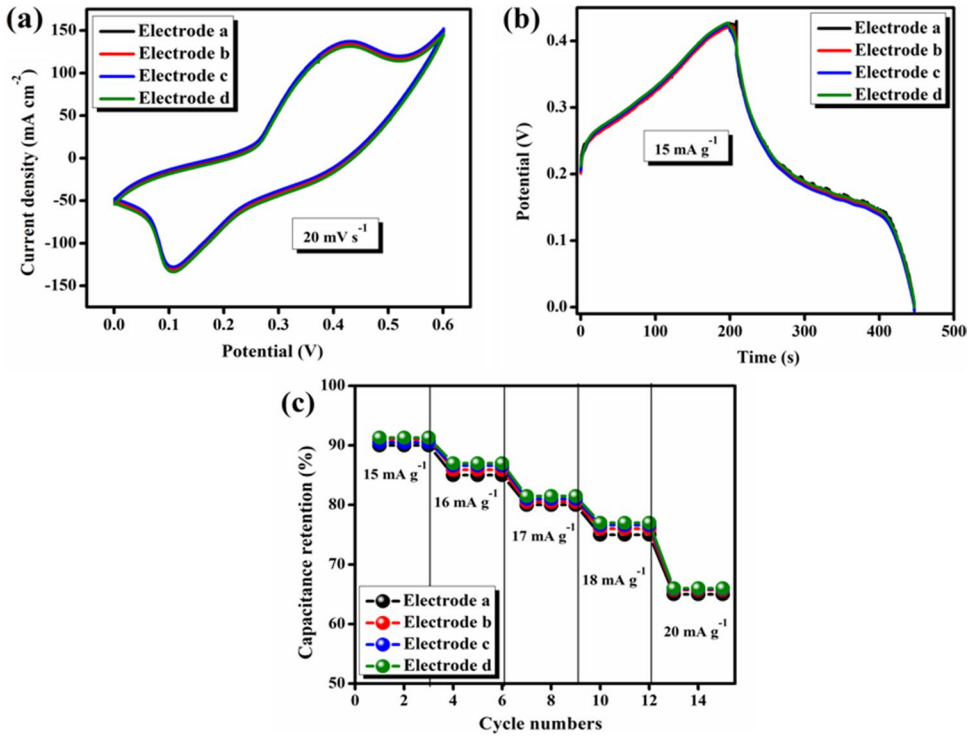

Fig. 11 Reproducibility test of (**a**) CV graphs of four electrodes taken at a scan rate of 20 mV s^{-1}, (**b**) GCD graphs of four electrodes at 15 mA g^{-1} current density, and (**c**) rate capability of the four electrodes at 15, 16, 17, 18 and 20 mA g^{-1} current density for three consecutive GCD cycles

analysis done in the frequency range from 100 kHz to 0.1 Hz depicted in Fig. 10 using three electrode systems. The Nyquist plots of all the sample electrodes possessed a small semicircle in high frequency region (Rct), which indicates lower charge-transfer resistance at the interface between the electrode/electrolyte. Also, a straight line nearer to the imaginary axis (Rs) with shorter length frequency, observed in the low frequency region, suggests low ion diffusion resistance from the electrolyte to the surface of the electrode (Ma et al. 2020). The calculated Rct values are displayed in Table 3.

Reproducibility analysis

The reproducibility of the performance of the best sample (NCR-3) was analyzed to evaluate the practical application of a supercapacitor. The as-fabricated four similar NCR-3 electrodes were named as electrode a, electrode b, electrode c and electrode d. The obtained CV at 20 mV s^{-1} scan rate and GCD curves at 15 mA g^{-1} current density of the four fabricated electrodes are depicted in Fig. 11a, b. The shape of the CV curves remains quasi-rectangular pattern for all the four prepared electrodes with least variation in the geometric area. The GCD curves remain almost similar in shape for all the four electrodes and possess excellent specific capacitance of 1597 F g^{-1}, 1590 F g^{-1}, 1583 F g^{-1} and 1575 F g^{-1} for electrode a, electrode b, electrode c, and electrode d, respectively, at current density of 15 mA g^{-1}. The slight variation in specific capacitance value might be due to the minor change in the loaded mass of each of the electrode samples as specific capacitance is inversely proportional to mass loading. The rate capability for the four NCR-3 electrodes is evaluated for three consecutive cycles at each current density of 15, 16, 17, 18 and 20 mA g^{-1} whose variation is depicted in Fig. 11c. Similar patterns are observed in the graph for three consecutive cycles for all the current densities. It is also found that the rate of change of capacitive response for all the four electrodes is almost same. These results indicate that the synthesized NCR-3 composite has good stability with high reproducibility (Sarmah and Kumar 2019; Li et al. 2011; Li et al. 2022).

Compared with pristine NC, the performance of rGO wrapped NCR-1, NCR-2 and NCR-3 samples possessed unique structure and morphology, which provides abundant electroactive sites. The higher rGO concentration helps in improving better stability, high contact area, and high electrochemical activity. The overall results illustrate that NCR-3 is a promising electrode material for supercapacitor applications, which exhibits satisfactory electrochemical behaviors, including high specific capacitance, good cycle stability, and high reproducibility.

Conclusion

The novel electrodes of pristine nickel copper sulfide and their composites with different concentrations of rGO nanosheets are synthesized using facile hydrothermal

technique. The synthesis procedure gives rise to rGO sheets wrapped β-phase$NiCu_2S$ nanorods, which is clear from XRD, FTIR, Raman, FESEM and XPS analysis. It is noted that GO is completely reduced to rGO during the synthesis of $NiCu_2S$/rGO composites. The electrochemical investigation states that the $NiCu_2S$/rGO composites perform better than pristine $NiCu_2S$ nanorods. Among different rGO composites, the $NiCu_2S$ nanorod composite with 0.15 wt.% of rGO exhibited high specific capacitance of 1583 F g^{-1} at 15 mA g^{-1} with excellent stability having capacitance retention of 89% after 5000 cycles possessing high reproducibility and rate capability.

Acknowledgements The authors thank to K.S. Rangasamy College of Technology for providing infrastructure to carry out this work. The authors also acknowledge to Sathyabama Institute of Science and Technology, Chennai, for providing the research support.

Author contribution Narthana Kandhasamy: methodology, creation of models, conducting research work, specifically performing experiments and data collections and writing—original draft. Preethi L.K.: methodology, formal analysis, writing—review and editing, supervision. Devendiran M.: formal analysis, validation. Lukasz Walczak: formal analysis, validation. Tom Mathews: validation, critical review, commentary and revision. Rajendran Venkatachalam: validation, formal analysis, critical review, commentary and revision, supervision.

Funding The authors thank the K.S. Rangasamy College of Technology, Tiruchengode; Indira Gandhi Centre for Atomic Research, Kalpakkam; and Sathyabama Institute of Science and Technology, Chennai, for providing research support for the part of synthesis and characterization studies carried out.

Data availability The data and materials analyzed in this study are included in this manuscript.

Declarations

Ethics approval Not applicable.

Consent to participate Not applicable.

Consent for publication Not applicable.

Competing interests The authors declare no competing interests.

References

Agboola PO, Shakir I, Almutairi ZA, Shar SS, Aboud MFA (2022) Carbon nanotubes fabricated Mn^{+2} doped CoS_2 composite-decorated on nickel foam as hybrid electrode material for supercapacitor applications. Physica b: Condens Matter 644:414211. https://doi.org/10.1016/j.physb.2022.414211

Antony RP, Preethi LK, Gupta B, Mathews T, Dash S, Tyagi AK (2015) Efficient electrocatalytic performance of thermally exfoliated reduced graphene oxide-Pt hybrid. Mater Res Bull 70:60–67. https://doi.org/10.1016/j.materresbull.2015.04.015

Alidoost M, Mangini A, Caldera F, Anceschi A, Amici J, Versaci D, Fagiolari L, Trotta F, Francia C, Bella F, Bodoardo S (2022) Micro-mesoporous carbons from cyclodextrin nanosponges enabling high-capacity silicon anodes and sulfur cathodes for lithiated Si-S batteries. Chem A Eur J 28(6):202104201. https://doi.org/10.1002/chem.202104201

Aloqayli S, Ranaweera C, Wang Z, Siam K, Kahol P, Tripathi P, Srivastava O, Gupta BK, Mishra S, Perez F (2017) Nanostructured cobalt oxide and cobalt sulfide for flexible, high performance and durable supercapacitors. Energy Storage Mater 8:68–76. https://doi.org/10.1016/j.ensm.2017.05.006

Arora R, Nehra SP, Lata S (2022) In-situ composited g-C_3N_4/polypyrrole nanomaterial applied as energy-storing electrode with ameliorated super-capacitive performance. Environ Sci Pollut Res 1-12. https://doi.org/10.1007/s11356-022-21777-8

Bandara TMWJ, Hansadi JMC, Bella F (2022) A review of textile dye-sensitized solar cells for wearable electronics. Ionics 28:2563–2583

Beigbaghlou SS, Kalbasi RJ, Marjani K, Habibi A (2018) Introducing of a new bio-inspired hierarchical porous silica as an inorganic host for Ni–Pd alloy nanoparticles for the synthesis of aminobiphenyls from the one-pot Suzuki-Miyaura coupling-nitro reduction. Catal Lett 148(8):2446–2458. https://doi.org/10.1007/s10562-018-2457-6

Bhagwan J, Hussain SK, Krishna BV, Yu JS (2020) β-NiS-3D microflower-based electrode for aqueous asymmetric supercapacitors. Sustain Energy Fuels 4(11):5550–5559. https://doi.org/10.1039/D0SE00780C

Bishop DW, Thomas PS, Ray AS (1998) Raman spectra of nickel (II) sulfide. Mater Res Bull 33(9):1303–1306. https://doi.org/10.1016/S0025-5408(98)00121-4

Boopathiraja R, Parthibavarman M, Prabhu S, Ramesh R (2020) A facile one step hydrothermal induced hexagonal shaped CuS/rGO nanocomposites for asymmetric supercapacitors. Mater Today: Proc 26:3507–3513. https://doi.org/10.1016/j.matpr.2019.06.006

Cao D, Cheng D (2019) One-pot synthesis of copper–nickel sulfide nanowires for overall water splitting in alkaline media. ChemComm 55(56):8154–8157. https://doi.org/10.1039/C9CC02977J

Chadha N, Sharma R, Saini P (2021) A new insight into the structural modulation of graphene oxide upon chemical reduction probed by Raman spectroscopy and X-ray diffraction. Carbon Lett 31(6):1125–1131. https://doi.org/10.1007/s42823-021-00234-5

Chen J, Xie J, Jia CQ, Song C, Hu J, Li H (2022) Economical preparation of high-performance activated carbon fiber papers as self-supporting supercapacitor electrodes. Chem Eng J 450:137938. https://doi.org/10.1016/j.cej.2022.137938

Dang A, Sun Y, Fang C, Li T, Liu X, Xia Y, Ye F, Zada A, Khan M (2022) Rational design of Ti_3C_2/carbon nanotubes/$MnCo_2S_4$ electrodes for symmetric supercapacitors with high energy storage. Appl Surf Sci 581:152432. https://doi.org/10.1016/j.apsusc.2022.152432

Darsara SA, Seifi M, Askari MB, Osquian M (2021) Hierarchical 3D starfish-like Ni_3S_4–NiS on reduced graphene oxide for high-performance supercapacitors. Ceram Int 47(15):20992–20998. https://doi.org/10.1016/j.ceramint.2021.04.099

Deng BL, Guo LP, Lu Y, Rong HB, Cheng DC (2022) Sulfur–nitrogen co-doped graphene supported cobalt–nickel sulfide rGO@ SN-$CoNi_2S_4$ as highly efficient bifunctional catalysts for hydrogen/oxygen evolution reactions. Rare Met 41(3):911–920

Gao W, Zhang Y, Wang Y, Xu J, Feng Y, Meng M, Sun L, Feng K, Yuan H, Liu K (2021) Nail-like Cu_2S nanoarrays with a partial interconnected structure synthesized on Cu foam for high-performance asymmetric supercapacitors. J Mater Sci: Mater Electron 32(16):21770–21779. https://doi.org/10.1007/s10854-021-06698-5

Gholami J, Arvand M (2021) Controlled synthesis of a hierarchical $CuNi_2O_4$@SnS nanocauliflower-like structure on rGO as a positive

electrode material for an asymmetric supercapacitor. New J Chem 45(34):15667–15675. https://doi.org/10.1039/D1NJ01508G

Ghosh K, Pumera M (2021) Free-standing electrochemically coated MoSx based 3D-printed nanocarbon electrode for solid-state supercapacitor application. Nanoscale 13(11):5744–5756. https://doi.org/10.1039/D0NR06479C

Ghosh S, Paul A, Samanta P, Landge B, Mandal SK, Sinha S, Dutta GG, Murmu NC, Kuila T (2021) Influence of transition metals (Cu and Co) on the carbon-coated nickel sulfide used as positive electrode material in hybrid supercapacitor device. J Compos Sci 5(7):180. https://doi.org/10.3390/jcs5070180

González PS, Colet LM (2019) Disinfection of naturally contaminated underground well water in an electrochemical cell with platinum/carbon black-based anodes. Environ Sci Pollut Res 5(4):399–403. https://doi.org/10.30799/jespr.184.19050405

Gou J, Xie S, Yang Z, Liu Y, Chen Y, Liu Y, Liu C (2017) A high-performance supercapacitor electrode material based on NiS/Ni_3S_4 composite. Electrochim Acta 229:299–305. https://doi.org/10.1016/j.electacta.2017.01.111

Guan B, Li Y, Yin B, Liu K, Wang D, Zhang H, Cheng C (2017) Synthesis of hierarchical NiS microflowers for high performance asymmetric supercapacitor. Chem Eng J 308:1165–1173. https://doi.org/10.1016/j.cej.2016.10.016

Gurzęda B, Buchwald T, Nocuń M, Bąkowicz A, Krawczyk P (2017) Graphene material preparation through thermal treatment of graphite oxide electrochemically synthesized in aqueous sulfuric acid. RSC Adv 7(32):19904–19911. https://doi.org/10.1039/c7ra01678f

He Y, Zhang X, Wang S, Meng J, Sui Y, Wei F, Qi J, Meng Q, Ren Y, Zhuang D (2020) Rubik's cube-like Ni_3S_4/CuS_2 nanocomposite for high-performance supercapacitors. J Alloys Compd 847:156312. https://doi.org/10.1016/j.jallcom.2020.156312

Hengne AM, Samal AK, Enakonda LR, Harb M, Gevers LE, Anjum DH, Hedhili MN, Saih Y, Huang KW, Basset JM (2018) Ni–Sn-supported ZrO_2 catalysts modified by indium for selective CO_2 hydrogenation to methanol. ACS Omega 3(4):3688–3701. https://doi.org/10.1021/acsomega.8b00211

Hidayah NMS, Liu WW, Lai CW, Noriman NZ, Khe CS, Hashim U, Lee HC (2017) Comparison on graphite, graphene oxide and reduced graphene oxide: synthesis and characterization. In AIP Conf Proc 1:150002

Hoa NV, Dat PA, Chi NV (2021) A hierarchical porous aerogel nanocomposite of graphene/$NiCo_2S_4$ as an active electrode material for supercapacitors. J Sci: Adv Mater Dev 6(4):569–577. https://doi.org/10.1016/j.jsamd.2021.07.007

Hsu SY, Hsu FH, Chen JL, Cheng YS, Chen JM, Lu KT (2021) The supercapacitor electrode properties and energy storage mechanism of binary transition metal sulfide $MnCo_2S_4$ compared with oxide $MnCo_2O_4$studied using in situ quick X-ray absorption spectroscopy. Mater Chem Front 5(13):4937–4949. https://doi.org/10.1039/D1QM00222H

Hu Q, Zhang S, Chen F, Li W, Jiangyu H, Liang X, Xiang B, Chen C, Zou X (2021) Controlled synthesis of a high-performance α-NiS/Ni_3S_4 hybrid by a binary synergy of sulfur sources for supercapacitor. J Colloid Interface Sci 581:56–65. https://doi.org/10.1016/j.jcis.2020.07.129

Hu Q, Zou X, Huang Y, Wei Y, Chen F, Xiang B, Wu Q, Li W (2020) Graphene oxide-drove transformation of NiS/Ni_3S_4 microbars towards Ni_3S_4 polyhedrons for supercapacitor. J Colloid Interface Sci 559:115–123. https://doi.org/10.1016/j.jcis.2019.10.010

Huang T, Qiu Z, Hu Z, Zhang Z (2021) Facile synthesis of porous rod-like $CuCo_2O_4$ nano-materials for high energy density asymmetric supercapacitors. Ionics 27(10):4473–4482. https://doi.org/10.1007/s11581-021-04191-x

Iqbal MF, Ashiq MN, Zhang M (2021a) Design of metals sulfides with carbon materials for supercapacitor applications: a review. Energy Technol 9(4):2000987. https://doi.org/10.1002/ente.202000987

Iqbal MF, Yousef AK, Hassan A, Hussain S, Ashiq MN, Razaq A (2021b) Significantly improved electrochemical characteristics of nickel sulfide nanoplates using graphene oxide thin film for supercapacitor applications. Jenergy Storage 33:102091. https://doi.org/10.1016/j.est.2020.102091

Iqbal MZ, Khan J, Gul A, Siddique S, Alzaid M, Saleem M, Iqbal MJ (2021c) Copper doped cobalt-manganese phosphate ternary composites for high-performance supercapattery devices. J Energy Storage 35:102307. https://doi.org/10.1016/j.est.2021.102307

Jansi RB, Dhivya N, Ravi G, Zance SS, Yuvakkumar R, Hong SI (2019) Electrochemical performance of β-Nis@$Ni(OH)_2$ nanocomposite for water splitting applications. ACS Omega 4(6):10302–10310

Justin AS, Vickraman P, Reddy BJ (2019) Carbon sphere@nickel sulfide core-shell nanocomposite for high performance supercapacitor application. Curr Appl Phys 19(3):295–302. https://doi.org/10.1016/j.cap.2018.12.010

Kamalanathan M, Gopalakrishnan R (2015) Electrostatic super coupling in copper sulphide (Cu_2S)-reduced graphene oxide composite and their enhanced optical characteristics. AIP Conf Proc 15(1665):120038

Kang C, Ma L, Chen Y, Fu L, Hu Q, Zhou C, Liu Q (2022) Metal-organic framework derived hollow rod-like NiCoMn ternary metal sulfide for high-performance asymmetric supercapacitors. Chem Eng J 427:131003. https://doi.org/10.1016/j.cej.2021.131003

Kar P, Farsinezhad S, Zhang X, Shankar K (2014) Anodic Cu_2S and CuS nanorod and nanowall arrays: preparation, properties and application in CO_2 photoreduction. Nanoscale 6(23):14305–14318. https://doi.org/10.1039/C4NR05371K

Karade SS, Dubal DP, Sankapal BR (2016) MoS_2 ultrathin nanoflakes for high performance supercapacitors: room temperature chemical bath deposition (CBD). RSC Adv 6(45):39159–39165. https://doi.org/10.1039/C6RA04441G

Karanfil G, Coskun H, Karakıs M, Sarilmaz A, Gencer A, Surucu G, Aljabour A, Ozel F (2022) Exploration of carbon additives to the synthesis of Cu2Mo6S8 structures and their electrocatalytic activity in oxygen reduction reaction. Int J Hydrog Energy 47(8):5326–5336. https://doi.org/10.1016/j.ijhydene.2021.11.180

Khanam Z, Liu J, Song S (2020) Flexible graphene paper electrode prepared via polyvinyl alcohol-assisted shear exfoliation for all-solid-state polymer supercapacitor application. Electrochim Acta 363:137208. https://doi.org/10.1016/j.electacta.2020.137208

Khani H, Wipf DO (2017) Iron oxide nanosheets and pulse-electrodeposited Ni–Co–S nanoflake arrays for high-performance charge storage. ACS Appl Mater Interfaces 9(8):6967–6978. https://doi.org/10.1021/acsami.6b11498

Kiey SAA, Hasanin MS (2021) Green and facile synthesis of nickel oxide-porous carbon composite as improved electrochemical electrodes for supercapacitor application from banana peel waste. Environ Sci Pollut Res 28(2021):66888–66900. https://doi.org/10.1007/s11356-021-15276-5

Lai C, Wu Q, Chen J, Wen L, Ren S (2010) Large-area aligned branched Cu_2S nanostructure arrays: room-temperature synthesis and growth mechanism. Nanotechnology 21(21):215602

Li H, Chai L, Wang X, Wu X, Xi G, Liu Y, Qian Y (2007) Hydrothermal growth and morphology modification of β-NiS three-dimensional flowerlike architectures. Cryst Growth Des 7(9):1918–1922. https://doi.org/10.1021/cg0703588

Li H, He Y, Dai Y, Ren Y, Gao T, Zhou G (2022) Bimetallic SnS_2/NiS_2@S-rGO nanocomposite with hierarchical flower-like architecture for superior high rate and ultra-stable half/full sodium-ion batteries. Chem Eng J 427:131784. https://doi.org/10.1016/j.cej.2021.131784

Li J, Xie H, Li Y, Liu J, Li Z (2011) Electrochemical properties of graphene nanosheets/polyaniline nanofibers composites as electrode for supercapacitors. J Power Sources 196(24):10775–10781

Li X, Yan W, Guo S, Liu Y, Niu J, Yin L, Wang Z (2021a) One-step electrochemical controllable preparation of nickel cobalt sulfide nanosheets and its application in supercapacitors. Electrochim Acta 387:138488. https://doi.org/10.1016/j.electacta.2021.138488

Li L, Zhang D, Deng J, Gou Y, Fang J, Cui H, Zhao Y, Cao M (2021b) Carbon-based materials for fast charging lithium-ion batteries. Carbon 183:721–734. https://doi.org/10.1016/j.carbon.2021.07.053

Lin S, Tang J, Zhang K, Suzuki TS, Wei Q, Mukaida M, Zhang Y, Mamiya H, Yu X, Qin LC (2021) High-rate supercapacitor using magnetically aligned graphene. J Power Sources 482:228995. https://doi.org/10.1016/j.jpowsour.2020.228995

Liu S, Mao C, Niu Y, Yi F, Hou J, Lu S, Jiang J, Xu M, Li C (2015) Facile synthesis of novel networked ultralong cobalt sulfide nanotubes and its application in supercapacitors. ACS Appl Mater Interfaces 7(46):25568–25573. https://doi.org/10.1021/acsami.5b08716

Liu W, Niu H, Yang J, Cheng K, Ye K, Zhu K, Wang G, Cao D, Yan J (2018) Ternary transition metal sulfides embedded in graphene nanosheets as both the anode and cathode for high-performance asymmetric supercapacitors Chemistry of Materials. Chem Mater 30(3):1055–1068. https://doi.org/10.1021/acs.chemmater.7b04976

Liu Q, Yang G, Li X, Zhang S, Chen R, Wang X, Gao Y, Wang Z, Chen L (2022) Polymer electrolytes based on interactions between [solvent-Li+] complex and solvent-modified polymer. Energy Stor Mater 51:443–452. https://doi.org/10.1016/j.ensm.2022.06.040

Liu R, Zhou A, Zhang X, Mu J, Che H, Wang Y, Wang T, Zhang Z, Kou Z (2021) Fundamentals, advances and challenges of transition metal compounds-based supercapacitors. Chem Eng J 412:128611. https://doi.org/10.1016/j.cej.2021.128611

Ma Y, Hao J, Liu H, Shi W, Lian J (2020) Facile synthesis clusters of sheet-like Ni_3S_4/CuS nanohybrids with ultrahigh supercapacitor performance. J Solid State Chem 282:121088. https://doi.org/10.1016/j.jssc.2019.121088

Maity CK, Goswami N, Verma K, Sahoo S, Nayak GC (2020) A facile synthesis of boron nitride supported zinc cobalt sulfide nano hybrid as high-performance pseudocapacitive electrode material for asymmetric supercapacitors. J Energy Storage 32:101993. https://doi.org/10.1016/j.est.2020.101993

Miao Y, Zhang X, Zhan J, Sui Y, Qi J, Wei F, Meng Q, He Y, Ren Y, Zhan Z (2020) Hierarchical NiS@CoS with controllable core-shell structure by two-step strategy for supercapacitor electrodes. Adv Mater Interfaces 7(3):1901618. https://doi.org/10.1002/admi.201901618

Murugadoss G, Kanda H, Tanaka S, Nishino H, Ito S, Imahori H, Umeyama T (2016) An efficient electron transport material of tin oxide for planar structure perovskite solar cells. J Power Sources 307:891–897. https://doi.org/10.1016/j.jpowsour.2016.01.044

Murugadoss G, Thangamuthu R, Jayavel R, Kumar MR (2015) Narrow with tunable optical band gap of CdS based core shell nanoparticles: applications in pollutant degradation and solar cells. J Lumin 165:30–39. https://doi.org/10.1016/j.jlumin.2015.03.036

Nandhini S, Muralidharan G (2021) Graphene encapsulated NiS/Ni_3S_4 mesoporous nanostructure: a superlative high energy supercapacitor device with excellent cycling performance. Electrochim Acta 365:137367. https://doi.org/10.1016/j.electacta.2020.137367

Narthana K, Durai G, Kuppusami P, Theerthagiri J, Sujatha S, Lee SJ, Choi MY (2021) One-step synthesis of hierarchical structured nickel copper sulfide nanorods with improved electrochemical supercapacitor properties. Int J Energy Res 45(7):9983–9998. https://doi.org/10.1002/er.6492

Ndambakuwa W, Ndambakuwa Y, Choi J, Fernando G, Neupane D, Mishra SR, Perez F, Gupta RK (2021) Nanostructured nickel-cobalt oxide and sulfide for applications in supercapacitors and green energy production using waste water. Surf Coat Technol 410:126933. https://doi.org/10.1016/j.surfcoat.2021.126933

Niu W, Xiao Z, Wang S, Zhai S, Qin L, Zhao Z, An Q (2021) Synthesis of nickel sulfide-supported on porous carbon from a natural seaweed-derived polysaccharide for high-performance supercapacitors. J Alloys Compd 853:157123

Ojha A, Tiwary D, Oraon R, Singh P (2021) Degradations of endocrine-disrupting chemicals and pharmaceutical compounds in wastewater with carbon-based nanomaterials: a critical review. Environ Sci Pollut Res 28(24):30573–30594. https://doi.org/10.1007/s11356-021-13939-x

Oliveira EHCD, Fraga DMDSM, Silva MPD, Fraga TJM, Carvalho MN, Freire EMPDL, Ghislandi MG, Sobrinho MADM (2019) Removal of toxic dyes from aqueous solution by adsorption onto highly recyclable xGnP®graphite nanoplatelets. J Environ Chem Eng 7:103001. https://doi.org/10.1016/j.jece.2019.103001

Patil AM, An X, Li S, Yue X, Du X, Yoshida A, Hao X, Abudula A, Guan G (2021) Fabrication of three-dimensionally hetero structured rGO/$WO_3$0.5H_2O@Cu_2S electrodes for high-energy solid-state pouch-type asymmetric supercapacitor. Chem Eng J 403:126411. https://doi.org/10.1016/j.cej.2020.126411

Peng W, Song N, Su Z, Wang J, Chen K, Li S, Wei B, Luo S, Xie A (2022) Two-dimensional MoS2/Mn-MOF/multi-walled carbon nanotubes composite material for high-performance supercapacitors. Microchem J 179:107506. https://doi.org/10.1016/j.microc.2022.107506

Perera SD, Mariano RG, Vu K, Nour N, Seitz O, Chabal Y, Balkus KJ (2012) Hydrothermal synthesis of graphene-TiO_2 nanotube composites with enhanced photocatalytic activity. ACS Catal 2:949–956. https://doi.org/10.1021/cs200621c

Pujari R, Lokhande A, Yadav A, Kim J, Lokhande C (2016) Synthesis of MnS microfibers for high performance flexible supercapacitors. Mater Des 108:510–517. https://doi.org/10.1016/j.matdes.2016.07.038

Purabgola A, Mayilswamy N, Kandasubramanian B (2022) Graphene-based TiO_2 composites for photocatalysis & environmental remediation: synthesis and progress. Environ Sci Pollut Res 29:32305–32325. https://doi.org/10.1007/s11356-022-18983-9

Rahaman S, Singha MK, Sunil MA, Ghosh K (2020) Effect of copper concentration on CTS thin films for solar cell absorber layer and photocatalysis applications. Superlattices Microstruct 145:106589. https://doi.org/10.1016/j.spmi.2020.106589

Ramesh S, Karuppasamy K, Vikraman D, Yadav HM, Kim HS, Sivasamy A, Kim HS (2022) Fabrication of $NiCo_2S_4$ accumulated on metal organic framework nanostructured with multi-walled carbon nanotubes composite material for supercapacitor application. Ceram Int 48:29102–29110. https://doi.org/10.1016/j.ceramint.2022.05.048

Rana U, Aman S, Ashiq MN, Iqbal MF, Manzoor S, Mahmoud MHH, Alhadhrami A, Elansry HO, El-Ansari DO, Taha TA (2022) Outstanding electrochemical behavior of reduced graphene oxide wrapped chromium sulfide nanoplates directly grown on nickel foam for supercapacitor applications. J Sol-Gel Sci Technol 103(3):704–712. https://doi.org/10.1007/s10971-022-05888-9

Rao R, Podila R, Tsuchikawa R, Katoch J, Tishler D, Rao AM, Ishigami M (2011) Effects of layer stacking on the combination Raman modes in graphene. ACS Nano 5(3):1594–1599. https://doi.org/10.1021/nn1031017

Reina M, Scalia A, Auxilia G, Fontana M, Bella F, Ferrero S, Lamberti A (2022) Boosting electric double layer capacitance in laser-induced graphene-based supercapacitors. Adv Sustain Syst 6(1):2100228. https://doi.org/10.1002/adsu.202100228

Sabeeh H, Aadil M, Zulfiqar S, Ayeman I, Shakir I, Agboola PO, Haider S, Warsi MF (2021) Self-supporting design of NiS/CNTs nanohybrid for advanced electrochemical energy storage applications. J Clust Sci 1-9.https://doi.org/10.1007/s10876-021-02138-w

Sarmah D, Kumar A (2019) Ion beam modified molybdenum disulfide-reduced graphene oxide/polypyrrole nanotubes ternary nanocomposite for hybrid supercapacitor electrode. Electrochim Acta 312:392–410

Shah P, Joshi K, Shah M, Unnarkat A, Patel FJ (2022) Photocatalytic dye degradation using nickel ferrite spinel and its nanocomposite. Environ Sci Pollut Res. https://doi.org/10.1007/s11356-022-21248-0

Shen J, Shi M, Yan B, Ma H, Li N, Ye M (2011) One-pot hydrothermal synthesis of Ag-reduced graphene oxide composite with ionic liquid. J Mater Chem 21(21):7795–7801. https://doi.org/10.1039/C1JM10671F

Shinde SK, Yadav HM, Ghodake GS, Jagadale AD, Jalak MB, Kim D-Y (2021) Novel and efficient hybrid supercapacitor of chemically synthesized quaternary 3D nanoflower-like $NiCuCo_2S_4$ electrode. Ceram Int 47(11):15639–15647. https://doi.org/10.1016/j.ceramint.2021.02.134

Shoeb M, Mobin M, Rauf MA, Adnan SM, Ansari SY (2021) Graphene nickel copper nanocomposite (Gr@NiCuNCs) as a binder free electrode for high energy density supercapacitor and antimicrobial application. Jmateriomics 7(4):815–827. https://doi.org/10.1016/j.jmat.2020.12.008

Shokry A, Karim M, Khalil M, Ebrahim S, Nady JE (2022) Supercapacitor based on polymeric binary composite of polythiophene and single-walled carbon nanotubes. Sci Rep 12(1):1–13

Siburian R, Sihotang H, Raja SL, Supeno M, Simanjuntak C (2018) New route to synthesize of graphene nano sheets. Orient J Chem 34(1):182

Singh WI, Sinha S, Devi NA, Nongthombam S, Laha S, Swain BP (2021) Investigation of chemical bonding and electronic network of rGO/PANI/PVA electrospun nanofiber. Polym Bull 78(11):6613–6629. https://doi.org/10.1007/s00289-020-03442-7

Singla MK, Nijhawan P, Oberoi AS (2021) Hydrogen fuel and fuel cell technology for cleaner future: a review. Environ Sci Pollut Res 28(13):15607–15626. https://doi.org/10.1007/s11356-020-12231-8

Tan P, Hu Y, Bi Q (2016) Competitive adsorption of Cu^{2+}, Cd^{2+} and Ni^{2+} from an aqueous solution on graphene oxide membranes. Colloids Surf APhysicochemEng Asp 509:56–64. https://doi.org/10.1016/j.colsurfa.2016.08.081

Tang Y, Chen T, Yu S (2015a) Morphology controlled synthesis of monodispersed manganese sulfide nanocrystals and their primary application in supercapacitors with high performances. ChemComm 51(43):9018–9021. https://doi.org/10.1039/C5CC01700A

Tang Y, Chen T, Yu S, Qiao Y, Mu S, Hu J, Gao F (2015b) Synthesis of graphene oxide anchored porous manganese sulfide nanocrystals via the nanoscale Kirkendall effect for supercapacitors. J Mater Chem A 3(24):12913–12919. https://doi.org/10.1039/C5TA02480C

Trikkaliotis DG, Mitropoulos AC, Kyzas GZ (2020) Low-cost route for top-down synthesis of over-and low-oxidized graphene oxide. Colloids Surf A Physico chemEng Asp 600:124928. https://doi.org/10.1016/j.colsurfa.2020.124928

Truong TT, Pham TT, Truong TTT, Pham TD (2022) Synthesis, characterization of novel ZnO/CuO nanoparticles, and the applications in photocatalytic performance for rhodamine B dye degradation. Environ Sci Pollut Res 29(15):22576–22588

Tung DT, Nguyet HM, Linh NTN, Dung NT, Quynh NV, Dang NV, Vernardou D, Le TK, Minh PN (2022) High electrochemical performance of ink solution based on manganese cobalt sulfide/reduced graphene oxide nano-composites for supercapacitor electrode materials. RSC Adv 12(31):20182–20190. https://doi.org/10.1039/D2RA02818B

Wang X, Li W, Xue Y, Liu J, Yue Y, Zhou C, Zhu K, Cao D, Chen Y, Wang G (2022) CoS/nitrogen-doped carbon composites derived from zeolitic imidazolate frameworks-67 as advanced electrodes for supercapacitors. J Energy Storage 50:104220. https://doi.org/10.1016/j.est.2022.104220

Wang F, Li G, Zheng J, Ma J, Yang C, Wang Q (2018) Microwave synthesis of three-dimensional nickel cobalt sulfide nanosheets grown on nickel foam for high-performance asymmetric supercapacitors. J Colloid Interface Sci 516:48–56. https://doi.org/10.1016/j.jcis.2018.01.038

Wang S, Wang J, Ji X, Meng J, Sui Y, Wei F, Qi J, Meng Q, Ren Y, He Y (2020a) Formation of hollow-cubic $Ni(OH)_2/CuS_2$ nanocomposite via sacrificial template method for high performance supercapacitors. J Mater Sci: Mater Electron 31(13):10489–10498. https://doi.org/10.1007/s10854-020-03597-z

Wang Y, Zhang W, Guo X, Liu Y, Zheng Y, Zhang M, Li R, Peng Z, Zhang Y, Zhang T (2020b) One-step microwave-hydrothermal preparation of NiS/rGO hybrid for high-performance symmetric solid-state supercapacitor. Appl Surf Sci 514:146080. https://doi.org/10.1016/j.apsusc.2020.146080

Wang Z, Su H, Liu F, Chu X, Yan C, Gu B, Huang H, Yang T, Chen N, Han Y (2019) Establishing highly-efficient surface faradaic reaction in flower-like $NiCo_2O_4$ nano-/micro-structures for next-generation supercapacitors. Electrochim Acta 307:302–309. https://doi.org/10.1016/j.electacta.2019.03.227

Wu Y, Yan M, Sun L, Shi W (2018) Flexible yolk-shelled $NiCo_2S_4$ hollow spheres/RGO film electrodes for efficient supercapacitive energy storage. New J Chem 42(19):16174–16182. https://doi.org/10.1039/C8NJ03049A

Xie X, Wu D, Feng X, Ni C, Sun X, Kimura H, Du W (2021) A novel (α-β) NiS/Ni_3S_4-rGO electrode material for supercapacitors. Colloids Interface Sci Commun 43:100453. https://doi.org/10.1016/j.colcom.2021.100453

Xu X, Liang L, Zhang X, Xing X, Zhao Y, Gao J, Wei A (2020) Design of reduced graphene oxide supported $NiMoS_4$ to enhance energy capacity of hybrid supercapacitors. Colloids Surf a: Physico chemEng Asp 586:124289. https://doi.org/10.1016/j.colsurfa.2019.124289

Xu Y, Liu X, Su H, Jiang S, Zhang J, Li D (2022a) Hierarchical bimetallic selenides $CoSe_2$–$MoSe_2$/rGO for sodium/potassium-ion batteries anode: insights into the intercalation and conversion mechanism. Energy Environ Mater 5(2):627–636. https://doi.org/10.1002/eem2.12206

Xu F, Zhao J, Wang J, Guan T, Li K (2022b) Strong coordination ability of sulfur with cobalt for facilitating scale-up synthesis of Co_9S_8 encapsulated S, N co-doped carbon as a trifunctional electrocatalyst for oxygen reduction reaction, oxygen and hydrogen evolution reaction. J Colloid Interface Sci 608:2623–2632. https://doi.org/10.1016/j.jcis.2021.10.182

Yibowei ME, Adekoya JG, Adediran AA, Adekomaya O (2021) Carbon-based nano-filler in polymeric composites for supercapacitor electrode materials: a review. Environ Sci Pollut Res 28(21):26269–26279. https://doi.org/10.1007/s11356-021-13589-z

Yoon IS, Kim CD, Min BK, Kim YK, Kim BS, Jung WS (2009) Characterization of graphene sheets formed by the reaction of carbon monoxide with aluminum sulfide. Bull Korean Chem Soc 30(12):3045–3048. https://doi.org/10.5012/bkcs.2009.30.12.3045

Yu Z, Li F, Di H, Pan Y, Lv L, Ma Y, Chen Q (2016) A facile one-pot method for preparation of the rGO-CuS/Cu_2S with enhanced photocatalytic activity under visible light irradiation. J Mater Sci: Mater Electron 27(5):5136–5144

Yue C, Li H, Shi H, Liu A, Guo Z, Mu J, Zhang X, Liu X, Che H (2021) Ag nanoparticles decorated CuS sub-micron flowers with enhanced energy storage performance for hybrid supercapacitors. J Alloys Compd 885:161080. https://doi.org/10.1016/j.jallcom.2021.161080

Zhai M, Li A, Hu J (2020) CuO nanorods grown vertically on graphene nanosheets as a battery-type material for high-performance

supercapacitor electrodes. RSC Adv 10(60):36554–36561. https://doi.org/10.1039/D0RA06758J

Zhang D, Gao S, Zhang J, Wang J, She W, Wang K, Xia X, Yang B, Meng X (2021a) Facile solid−phase synthesis of layered NiS/rGO nanocomposite for high−performance hybrid supercapacitor. J Power Sources 514:230590. https://doi.org/10.1016/j.jpowsour.2021.230590

Zhang G, Xuan H, Yang J, Wang R, Xie Z, Liang X, Han P, Wu Y (2021b) Preparation and characterization of Novel 2D/3D $NiSe_2$/MnSe grown on rGO/Ni foam for high-performance battery-supercapacitor hybrid devices. J Power Sources 506:230255. https://doi.org/10.1016/j.jpowsour.2021.230255

Zhang J, Zhang D, Yang B, Shi H, Wang K, Han L, Wang S, Wang Y (2020) Targeted synthesis of NiS and NiS_2 nanoparticles for high−performance hybrid supercapacitor via a facile green solid−phase synthesis route. J Energy Storage 32:101852. https://doi.org/10.1016/j.est.2020.101852

Zhang J, Liu J, Kang D, Su Z, Liang W, Zhi L (2021c) Facile synthesis of hierarchically porous carbon for supercapacitor derived from water-soluble pitch. IOP Conf Ser: Earth Environ Sci 631(1):012101. https://doi.org/10.1088/1755-1315/631/1/012101

Zhang M, Hu H, Qi J, Wei F, Meng Q, Ren Y, Zhan Z, Sui Y, Sun Z (2021d) Expeditious and controllable synthesis of micron flower-like architecture Cu_7S_4@ LSC via Ni ions morphology confinement for asymmetric button supercapacitor. Electrochim Acta 366:137362. https://doi.org/10.1016/j.electacta.2020.137362

Zhu G, Jin Y, Ge M (2022) Simple preparation of a CuO@γ-Al_2O_3 Fenton-like catalyst and its photocatalytic degradation function. Environ Sci Pollut Res 29:68636–68651. https://doi.org/10.1007/s11356-022-20698-w